HHS Public Access

Author manuscript

J Comp Neurol. Author manuscript; available in PMC 2017 May 27.

Published in final edited form as:

J Comp Neurol. 2015 October 15; 523(15): 2277–2296. doi:10.1002/cne.23789.

Convergence of Lemniscal and Local Excitatory Inputs on Large GABAergic Tectothalamic Neurons

Tetsufumi Ito[1,2], **Hiroyuki Hioki**[3], **Jaerin Sohn**[3,4], **Shinichiro Okamoto**[3], **Takeshi Kaneko**[3], **Satoshi Iino**[1,2], and **Douglas L. Oliver**[5]

[1]Department of Anatomy, Faculty of Medical Sciences, University of Fukui, Eiheiji, Fukui, 910-1193, Japan

[2]Research and Education Program for Life Science, University of Fukui, Fukui, Fukui, 910-8507, Japan

[3]Department of Morphological Brain Science, Graduate School of Medicine, Kyoto University, Yoshida-Konoe, Kyoto, 606-8501, Japan

[4]Research Fellow of Japan Society for the Promotion of Science (JSPS), 5-3-1 Koujimachi, Chiyoda-ku, Tokyo, 102-8472, Japan

[5]Department of Neuroscience, University of Connecticut Health Center, Farmington, CT, 06030-3401

Abstract

Large GABAergic (LG) neurons form a distinct cell type in the inferior colliculus (IC), identified by the presence of dense VGLUT2-containing axosomatic terminals. Although some of the axosomatic terminals originate from local and commissural IC neurons, it has been unclear whether LG neurons also receive axosomatic inputs from the lower auditory brainstem nuclei, i.e. cochlear nuclei (CN), superior olivary complex (SOC), and nuclei of the lateral lemniscus (NLL). In this study, we injected recombinant viral tracers that force infected cells to express GFP in a Golgi-like manner into the lower auditory brainstem nuclei to determine whether these nuclei directly innervate LG cell somata. Labeled axons from CN, SOC and NLL terminated as excitatory axosomatic endings, identified by co-labeling of GFP and VGLUT2, on single LG neurons in the IC. Each excitatory axon made only a few axosomatic contacts on each LG neuron. Inputs to a single LG cell are unlikely to be from a single brainstem nucleus, since lesions of individual nuclei failed to eliminate most VGLUT2-positive terminals on the LG neurons. The estimated number of inputs on a single LG cell body was almost proportional to the surface area of the cell body. Double injections of different viruses in IC and in a brainstem nucleus showed that LG neurons received inputs from both. These results demonstrated that both ascending and intrinsic sources converge on the LG somata to control inhibitory tectothalamic projections.

Corresponding Author: Tetsufumi Ito, Department of Anatomy, Faculty of Medical Sciences, University of Fukui, Eiheiji, Fukui, 910-1193, Japan, Telephone number: +81-776-61-8302, itot@u-fukui.ac.jp.

Conflict of interest: The authors declare no conflict of interest.

Author contributions: Study concept and design: TI and DLO. Acquisition of data: TI. Analysis and interpretation of data: TI and DLO. Drafting of the manuscript: TI, DLO, HH. Administrative, technical, and material support: HH, JS, SO, TK, SI. Statistical analysis: TI.

Graphical abstract

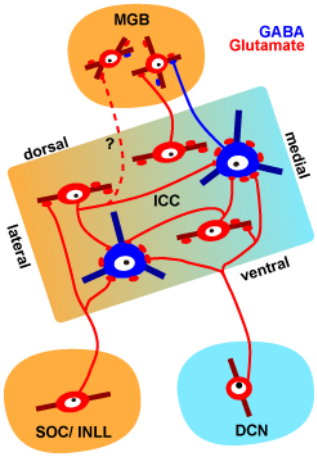

Keywords

inferior colliculus; vesicular glutamate transporter; GABA; auditory system; excitatory axosomatic synapse; RRID: AB_2278725; RRID: AB_94856; RRID: AB_94966; RGD ID: 1566430

Introduction

The inferior colliculus (IC) is a key midbrain center of the auditory system and receives inputs from virtually all lower auditory brainstem nuclei, i.e. cochlear nuclei (CN), superior olivary complex (SOC), and nuclei of the lateral lemniscus (NLL). In addition to the ascending lemniscal inputs, neighboring neurons in IC will influence each other since most IC neurons have local collaterals (Ito and Oliver, 2014; Oliver et al., 1991; Wallace et al., 2012). However, direct morphological evidence for the convergence of ascending and local inputs is lacking.

In the IC, large GABAergic (LG) neurons are tectothalamic neurons (Bartlett and Smith, 1999; Peruzzi et al., 1997; Winer et al., 1996), and are encircled by dense axosomatic excitatory inputs from presynaptic terminals that contain the vesicular glutamate transporter 2 (VGLUT2) (Geis and Borst, 2013; Ito et al., 2009; Ito and Oliver, 2012). To elucidate the function of LG neurons, it is important to establish the origin of the axosomatic terminals. Thus, our goal is to understand the origin of these terminals. We have begun by examining the origin of excitatory axosomatic terminals in experiments where the target neurons can be identified unambiguously. Previously, retrograde labeling demonstrated that the candidates of origins of VGLUT2-containing axosomatic terminals were the dorsal cochlear nucleus (DCN), SOC, intermediate nucleus of the lateral lemniscus (INLL), and IC (Ito and Oliver, 2010). While local and commissural IC neurons have been shown to make axosomatic excitatory synapses on the LG neurons (Ito and Oliver, 2014), it remains unclear whether the brainstem nuclei contribute similar axosomatic inputs.

In this study, we asked whether excitatory neurons in the lower auditory brainstem nuclei make axosomatic excitatory inputs on the LG neurons. We used recombinant viral vectors to

fill dendrites and axons with fluorescent proteins similar to a Golgi stain. We found that VGLUT2-positive (VGLUT2+) terminals from the CN, SOC, and NLL made axosomatic inputs on LG neurons. These inputs converged with inputs from local axons on the LG neurons. The results suggest that information conveyed by lemniscal fibers is modified by the local inputs on an LG cell body.

Materials and methods

Preparation of adeno-associated virus vector

For efficient labeling of neurons, we utilized Sindbis virus expressing palmitoylation site-attached GFP (palGFP, Furuta et al., 2001) or mRFP (pal-mRFP, Nishino et al., 2008) and adeno-associated virus vector newly prepared as described below.

We firstly amplified woodchuck hepatitis virus posttranscriptional regulatory element (WPRE, a gift from Dr. Hope, Zufferey et al., 1999) by polymerase chain reaction with the following primers: 5′-AAAACTCGAGACGCGTCGATAATCAACCTCTGGATT-3′ and 5′-TTTTAGATCTCGATGCGGGGAGGCGGCCCA-3′ (XhoI, MluI, and BglII sites underlined), and subcloned into XhoI and BglII sites of pAAV-MCS (Stratagene, La Jolla, CA), resulting in pAAV-MCSW. Then, palGFP sequence (Tamamaki et al., 2000) was amplified by polymerase chain reaction with the primers, 5′-AAAAAGATCTGCCACCATGCTGTGCTGTAT-3′ and 5′-TTTTCTCGAGTTACTTGTACAGCTCGTCCA-3′ (BglII and XhoI sites underlined), and inserted into BamHI and XhoI sites of pAAV-MCSW, resulting in pAAV-CMV-palGFP-WPRE.

The production and purification of the adeno-associated virus vector were performed according to a previous report (Kataoka et al., 2014) with some modifications. Briefly, 6 hours after co-transfection of vector and helper plasmids (pXR5, University of North Carolina at Chapel Hill; pHelper, Stratagene) into HEK293T cells (RCB2202, RIKEN BRC, Japan) by using polyethylenimine, the medium was replaced with virus production medium consisting of D-MEM (Invitrogen, Eugene, OR), 10% fetal bovine serum, 4 mM L-glutamine (Invitrogen), 2 mM GlutaMAX (Invitrogen), 0.1 M Non-Essential Amino Acids (Invitrogen), and 1 mM sodium pyruvate (Invitrogen). After 72 hours, the medium containing the viral particles was collected, ultracentrifuged with OptiPrep (Axis-Shield, Oslo, Norway), and concentrated with Amicon Ultra-15 (NMWL 50K; Millipore, Temecula, CA). Viral titers (transducing units/ml) were adjusted to 1.0×10^9 TU/ml, and the viral solution was stored in aliquots at −80°C until use for delivery to brain tissues.

Animals

Thirty-four Long-Evans rats (RGD ID: 1566430) of both sexes were used in this study. Of these, nineteen animals received viral injections (Table 1). Twelve animals received kainic acid injections. Three animals were normal controls. All experiments were conducted in accordance with institutional guidelines at the University of Fukui and the University of Connecticut Health Center. All efforts were made to minimize the number of animals used and their suffering.

Viral injections

Rats were anesthetized with a ketamine & xylazine mixture (97.6 mg/kg & 2.4 mg/kg, i.m.). After animals were positioned in a stereotaxic apparatus, one to four craniotomies were made in the parietal bone, and a glass micropipette with a tip diameter of 10~20 μm, filled with either palGFP Sindbis, pal-mRFP Sindbis, or adeno-associated virus 2/5-palGFP viral solutions, was advanced into the IC, SOC, DCN, or INLL. In 12 cases, the injection of the viral tracers was made in one of these nuclei (Table 1). In seven cases, the injection was made in 2 different locations in the same animal. Since INLL neurons project unilaterally in the rat (Ito and Oliver, 2010), we made injections in the INLL bilaterally and examined the IC of both sides in case 11-22. In five cases, palGFP Sindbis virus was injected bilaterally into the IC, and Sindbis pal-mRFP virus was injected bilaterally into the SOC (Table 1). A unilateral CN injection of Sindbis pal-mRFP was made in case 11-37 after bilateral IC injections of palGFP Sindbis. The viral solution (0.1–1.0 μl) was pressure-injected using nitrogen gas and a custom-made device.

After a survival period of 36–48 hours for Sindbis virus and 7 days for adeno-associated virus, rats were re-anesthetized with a ketamine & xylazine mixture and perfused transcardially with 4% paraformaldehyde in 0.1 M phosphate buffer (pH 7.4). After cryoprotection with 30% sucrose in 0.1 M phosphate buffer (pH 7.4) at 4 °C for 1–2 days, 40 μm-thick serial coronal sections of the brainstem were cut with a freezing microtome from the rostral medial geniculate body to a point caudal to the DCN. Every 6th section was temporarily mounted on non-coated glass slides, cover-slipped with 0.05 M phosphate-buffered saline, and examined under a fluorescent microscope (BX-51, Olympus Corporation, Tokyo, Japan) to confirm the injection site and to make a rough estimate of the number of infected neurons. After the examination, the sections were floated off gently from the glass slides with a wet brush, and stored in 0.05 M phosphate-buffered saline containing 2% sodium azide at 4 °C together with the other, non-examined sections.

Kainic acid injections

To make kainic acid injections, rats were anesthetized with a ketamine & xylazine mixture (97.6 mg/kg & 2.4 mg/kg i.m.), and maintained in areflexia with 1% isoflurane. Glass micropipettes (4–7 μm tip, 0.5–5 M Ω) were filled with 0.2% kainic acid diluted in saline. These glass electrodes were advanced through the cortex after the dura was opened. Short latency responses to white noise bursts or pure tones was used to locate auditory nuclei. After confirming that a tip of the electrode was in either the IC, NLL, SOC, or CN (3 cases each), pressure injections of 0.25–0.5 μl of 0.2% kainic acid were made with a Picospritzer (General Valve). After the surgery, 5 mg/kg of diazepam was injected intraperitoneally to prevent seizures induced by kainic acid.

Fourteen days after the surgery, the rats were deeply anesthetized with a ketamine & xylazine mixture, and perfused transcardially with 4% paraformaldehyde in 0.1 M phosphate buffer (pH 7.4). After cryoprotection in 30% sucrose in 0.1 M phosphate buffer (pH 7.4) for 2 days, serial, 20 μm-thick, coronal sections were cut with a freezing microtome. A series of every 12th section was used for histology.

Antibodies

In this study, mouse monoclonal antibodies were used for glutamic acid decarboxylase 67 (GAD67; antiserum MAB5406, Millipore, Billerica, MA, RRID: AB_2278725), MAP2 (clone AP20, MAB3418, Millipore, RRID: AB_94856), and NeuN (clone A60, MAB377, Millipore, RRID: AB_94966); rabbit polyclonal antibodies were used for VGLUT2 (Fujiyama et al., 2001), GFP (Tamamaki et al., 2000), and mRFP (Hioki et al., 2010); and guinea pig polyclonal antibodies were used for VGLUT2 (Fujiyama et al., 2001), GFP (Tamamaki et al., 2000), and mRFP (Hioki et al., 2010) (Table 2).

The immunogen used for anti-GAD67 antibody was a recombinant whole protein of rat GAD67. In the previous study (Ito et al., 2007), we confirmed the specificity of the anti-GAD67 by western blot and an absorption test. In the western blot, a single band around 67 kDa was detected (which is also described in manufacturer's sheet). No signal was detected in rat brain sections incubated with the antibody (1:3000) preabsorbed with recombinant rat GAD67 protein (180 μg/ml). Furthermore, the staining pattern of the antibody was consistent with that in a previous study (Mugnaini and Oertel, 1985).

The immunogen used for anti-MAP2 antibody was bovine brain microtubule protein (aa. 997–1332). MAP2 associates with microtubules, neurofilaments, and actin filaments and is confined to neuronal cell bodies and dendrites. In the western blot, a single band around 300 kDa was detected (manufacturer's data sheet, Papadeas et al., 2008).

The immunogen used for anti-NeuN antibody was purified cell nuclei from mouse brain. Only one NeuN clone exists (A60) and it reacts with an uncharacterized nuclear protein (according to manufacturer's data sheet). The antibody recognizes cell nuclei and cytoplasm in the most regions of brain. In the western blot, 2–3 bands around 46–48kDa were detected (manufacturer's data sheet, Mullen et al., 1992).

The immunogen used for anti-VGLUT2 antibody was a synthetic peptide to C-terminal amino acid residues CWPNGWEKKEEFVQESAQDAYSYKDRDDYS of rat VGLUT2 (aa. 554–582). Specificity for the antibody was characterized by western blot and an absorption test (Fujiyama et al., 2001). In the western blot, a single band around 62 kDa was detected. No signal was detected in rat brain sections incubated with antibody preabsorbed with 10000-fold (in mol) excess amounts of the synthetic peptide used for the immunization.

The immunogen used for anti-GFP antibody was a recombinant whole protein of enhanced green fluorescent protein. The immunogen used for anti-mRFP antibody was a recombinant whole protein of monomeric red fluorescent protein. The specificity of GFP and mRFP antibodies was confirmed by the absence of staining in a rat brain that did not receive viral injections.

Non-fluorescent immunohistochemistry

Sections were incubated overnight with either rabbit anti-GFP (0.2 μg/ml), rabbit anti-mRFP (0.2 μg/ml), guinea-pig anti-VGLUT2 (0.5μg/ml), mouse anti-MAP2 (1:200), or mouse anti-NeuN (1:100) diluted in incubation buffer (1% normal donkey serum, 0.3% Triton X-100, 0.2% sodium azide, and 0.05 M phosphate-buffered saline). The next day, sections were

washed and incubated for an hour with donkey biotinylated anti-rabbit, anti-guinea-pig, or anti-mouse IgG (1:200; Jackson Immunoresearch, West Grove, PA) followed by an incubation for 1 hour with avidin-biotinylated horseradish peroxidase complex (1:50; ABC Elite, Vector Laboratories, Burlingame, CA). Bound peroxidase was visualized as a dark blue stain with a nickel-diaminobenzidine reaction. The sections were mounted on coated glass slides, counterstained with Neutral-Red (Merck, Whitehouse Station, NJ), dehydrated, cleared with xylene, and cover-slipped with Entellan (Merck).

Immunofluorescent labeling

Sections were incubated overnight with mouse anti-GAD67 (1:1000), guinea pig anti-VGLUT2 (0.5 μg/ml), and rabbit anti-GFP (0.5 μg/ml) diluted in incubation buffer. The next day, sections were washed and incubated for 3 hours with donkey AlexaFluor488-conjugated anti-rabbit IgG (1:200; Life Technologies), Cy3-conjugated anti-guinea pig IgG (1:200; Jackson), and Cy5-conjugated anti-mouse IgG (1:200; Jackson). Sections were mounted on coated glass slides, air dried, rehydrated, and cover-slipped with 1,4-diazabicyclo[2.2.2]octane.

In the six cases that received injections of palGFP and pal-mRFP Sindbis viruses, sections were incubated overnight with mouse anti-MAP2 (1:200), guinea pig anti-VGLUT2 (0.5 μg/ml), and rabbit anti-mRFP (0.5 μg/ml) diluted in incubation buffer. The next day, sections were washed and incubated with donkey DyLight 405-conjugated anti-mouse IgG (1:100; Jackson), Cy3-conjugated anti-rabbit IgG (Jackson), and Cy5-conjugated anti-guinea pig IgG (Jackson) for 3 hours. Sections were mounted on coated glass slides, air dried, rehydrated, and cover-slipped with 1,4-diazabicyclo[2.2.2]octane.

Imaging of fluorescent materials

Fluorescent micrographs were acquired with a confocal scanning laser microscope (TCS AOBS SP2, Leica Microsystems, Wetzlar, Germany). GFP and AlexaFluor488 were excited by a 488 nm Ar laser, and emitted fluorescence was filtered with a 500–530 nm band-pass filter. Cy3 was excited by a 543 nm He-Ne laser, and emitted fluorescence was filtered with a 565–615 nm band-pass filter. Cy5 was excited by a 633 nm He-Ne laser, and emitted fluorescence was filtered with a 650 nm low-pass filter. Z-stack images of each dye were taken sequentially to avoid bleed-through artifact. The image stacks were deconvoluted to remove out-of-focus signals with Huygens Essential software (Scientific Volume Imaging, Hilversum, Netherlands). Minimal adjustments of the fluorescent intensity levels were made on the deconvoluted images in Photoshop CS3 (Adobe Systems, San Jose, CA).

Analysis of terminals in fluorescent images

Images of LG neurons were acquired with a confocal scanning laser microscope with a ×63 oil-immersion lens (NA = 1.4). For imaging terminal contacts on cell bodies, we took Z-stack images at ×32 optical zoom, which is the maximal magnification of the system, at a z-interval of 113 nm. Deconvoluted fluorescent image stacks were analyzed and visualized with custom-made software written in MATLAB (Mathworks, Natick, MA). Z-stack high-magnification images of LG cells and their surrounding structures were analyzed for the termination of a single axon. The Z-stacks contained 1–3 separate axons. If an axon branch

terminated on an LG cell body, the axon swellings on the cell body were defined as "terminal boutons". If an axon branch passed by an LG cell body and the axon's swellings made contact on the cell body, the swellings were defined as "*en passant* varicosities". The number of contacts of both categories was counted for each separate axon. Three-dimensional reconstructions of single axons and cell bodies of LG cells were made from the Z-stacks, and the volume of GFP-positive (GFP+) terminals and surface area of LG cell bodies were calculated from the reconstructions. The number of axosomatic inputs was estimated by dividing total number of axosomatic VGLUT2-positive (VGLUT2+) terminals by number of axosomatic terminals which arose from a single axon or all axons in the stack and were positive for both GFP and VGLUT2 (GFP+/VGLUT2+).

To estimate the relationship between surface area of LG cell bodies and number of inputs, a generalized linear model was employed. Since the number of inputs takes continuous positive values, we assumed that the number obeys a gamma distribution. We hypothesized that the surface area (x) and number of inputs (y) increase monotonically and thus obey:

$$y = A\,x^{b}$$

Parameters of the model was estimated with R software (version 2.15.2; http://www.r-project.org/). The model was validated by comparing Akaike's information criteria (Akaike, 1973) with linear and null models.

Analysis of injection sites

Injection sites of recombinant viruses were drawn from bright field specimens with Neurolucida software (MBF Bioscience, Williston, VT). Z-stack images of the injection sites were acquired from a second series of sections labeled with fluorescent dyes using a confocal scanning laser microscope and a ×20 objective lens (NA = 0.5). We were able to distinguish GFP+ neurons from GFP+ glial cells by examining the morphology of their processes in Z-stack images. The fluorescent images of the injection sites were superimposed on the Neurolucida trace, and the cell bodies of GFP+ neurons were plotted. In some cases, the images of the center of the injection sites were too crowded by GFP+ cells to distinguish neurons and glial cells. In such cases, Z-stack images of the injection sites were imaged again with ×40 oil-immersive lens (NA = 1.25), and only cells with clear dendrites were counted as neurons while cells with ambiguous morphology were not counted.

Injection sites of kainic acid were drawn with Neurolucida from sections counterstained with Neutral-Red. Neighboring sections immunostained for MAP2 or NeuN were also examined to confirm the lesion sites.

Stereological analysis

In the kainic acid injection cases (N = 12) and in three control cases, the number of LG cells was counted with stereological methods using Stereo Investigator software (MBF Bioscience). IC sections were divided into a 300 × 300 μm grid, with a 50 × 50 × 20 μm box in the left-top of the grid as a sampling frame with 2 inclusion lines and 2 exclusion lines.

The top and bottom 2 μm of the section were reserved as guard zones. Nissl-stained cells with dense VGLUT2+ axosomatic endings (“axosomatic rings”) were counted if they were found between guard zones and did not intersect the exclusion lines. The mean number of LG cells per a sampling frame was calculated by dividing total number of LG cells by the total number of sampling frames (312 mean sampling frames, N = 15). The neural density within the kainic acid lesion site was estimated in similar manner (338 mean sampling frames, N = 12). MAP2 or NeuN stained cell bodies in the injected sites were counted and compared to those in intact nuclei.

Spatial distribution of LG cell bodies

To analyze the spatial distribution of LG cells that received axosomatic contacts from terminals positive for both GFP and VGLUT2, we re-scanned a series of every 6th section from 11 rats (10-60, 10-61, 11-49, 13-66 for SOC, 10-66, 10-67, 10-68 for CN, and 11-09, 11-22, 13-80, 14-16 for NLL injection). First, images covering the whole IC were acquired with a ×20 objective lens, and low-magnification montages of IC sections were made. Next, the IC was examined with a fluorescent microscope attached to a confocal scanning laser microscope. If GFP+ terminals were found in the field of view, Z-stack images from the top to bottom of the section were taken with the confocal scanning laser microscope with a ×40 oil-immersion lens (NA = 1.25) at a voxel size of 0.366 × 0.366 × 1 μm. The maximal projection of the Z-stack images were superimposed on the low-magnification montages. If we found LG cell bodies receiving axosomatic contacts with GFP+/VGLUT2+ terminals, we plotted the loci of the cell bodies on the montages. The raw montages and the montages with plots of LG cell bodies were both imported to Neurolucida software. Subdivisions of the IC were drawn from the VGLUT2 and GAD67 staining pattern in the montage and neighboring Neutral-Red-stained sections. All statistical analyses were done with R software and custom-made scripts.

Results

Lower auditory nuclei make excitatory axosomatic contacts on LG cells

SOC injection cases—After large injections of the palGFP Sindbis or adeno-associated virus 2/5 palGFP viral solution into the SOC (Fig. 1A; Table 3), many olivary neurons were infected as were a few in the non-auditory nuclei dorsal to the SOC. Labeled neurons were abundant in the medial superior olive (MSO) and surrounding periolivary nuclei (i.e. ventromedial, dorsal, and rostral periolivary nuclei, and lateral and ventral nuclei of the trapezoid body). Fewer neurons were labeled in the lateral superior olive (LSO) (Table 3). In the MSO, most labeled neurons were negative for GAD67. In case 10-60, neurons in dorsal MSO were labeled, whereas in cases 10-61 and 11-49 labeled MSO neurons were mainly located in the ventral part. In case 13-66, labeled MSO neurons were distributed throughout the nucleus. Colocalization of GFP and GAD67 was more common in neurons of the periolivary nuclei. In case 11-49, an injection was made in the more medial part of the SOC, and all the labeled periolivary neurons were located medial to the MSO. In cases 10-60, 10-61, and 13-66, labeled periolivary neurons were found both lateral and medial to the MSO. In case 13-66, both GAD67-positive (GAD67+) and −negative (GAD67−) LSO neurons were infected. Although it is widely accepted that inhibitory neurons in the LSO are

glycinergic (e.g. Saint Marie and Baker, 1990), GABA has been shown to be present in the cell bodies of these neurons (Magnusson et al., 2008), and most glycinergic LSO neurons co-express GAD67 and vice versa (Tanaka and Ezure, 2004). Therefore, it is presumed that GAD67+ neurons are glycinergic whereas GAD67− neurons are glutamatergic. GFP+ neurons without GAD67 immunoreactivity (GFP+/GAD67−) were sparsely distributed throughout the LSO with no clear medio-lateral bias.

In the IC, GFP+ axons from the superior olive were found bilaterally in cases 10-60, 10-61 and 13-66, and ipsilaterally in case 11-49. These axons made dense terminal plexuses in the ICC. Terminals of GFP+ axons containing VGLUT2, GAD67, or neither, were likely to represent glutamatergic, GABAergic, and glycinergic phenotypes, respectively. Superior olivary terminals containing both GFP and VGLUT2 (GFP+/VGLUT2+) made contacts on LG cell bodies and dendrites in the ipsilateral and contralateral IC of all cases except for case 11-49 where these inputs were only found in the contralateral IC. The majority of LG cells receiving GFP+/VGLUT2+ axosomatic contacts were found in the ICC, and fewer LG cells with these contacts were in the brachial nucleus of the IC (BIC), the rostral (ICR), lateral (ICL), or dorsal (ICD) cortex of IC (Fig. 2A; Table 3). Inside the ICC, the LG cells receiving axosomatic contacts tended to be in the lateral part. In case 10-61, LG neurons receiving labeled terminals were found mainly in the ventral part of the ICC. In other cases, LG neurons receiving labeled terminals were not concentrated in specific part of the dorso-ventral axis. For 11 LG cells, the axosomatic contact was confirmed by deconvoluted Z-stack images that contained both LG somata and GFP+/VGLUT2+ terminals (Fig. 3A–D). Here, and in the following figures, the double labeling is seen in 3 views: A single image in the original plane of section and two side views of the Z-stack that are shown above and to the right of the image in the normal plane (Fig. 3B$_2$–**B$_3$**, **D$_2$–D$_3$)**. Both the GFP+ and VGLUT2+ profiles matched in all three views indicating that the 2 molecules were colocalized rather than separated in different Z-positions.

CN injection cases—After large injections of the virus into the CN (Table 1), GFP+ neurons were found in the DCN, anteroventral and posteroventral cochlear nuclei (AVCN; PVCN) (Fig. 1B; Table 4). In case 10-66 and 10-68, the injections were made in the medial or rostromedial parts of the CN, respectively, while the injection in case 10-67 was made in the caudolateral part of the DCN. Therefore, case 10-67 involved the low frequency part of the DCN, while 10-66 involved the high frequency part according to the DCN frequency map of cats (Spirou et al., 1993). Both GAD67+ and GAD67− neurons were infected with the virus. In the DCN, large, GAD67− neurons (filled squares in Fig. 1B) were found in layer 2 and 3 of the DCN, and they were presumably fusiform and giant cells, respectively (Young and Oertel, 2004). Small GFP+/GAD67− neurons were identified as granule cells (dots in Fig. 1B). The DCN is known to contain 2 types of inhibitory neurons, i.e. cartwheel and vertical cells (Young and Oertel, 2004). Some of the GFP+ cells in layer 2 had highly branched dendrites in layer 1, and were likely to be cartwheel cells. All of them were GAD67+, as also shown in a previous study (Kemmer and Vater, 2001). We did not find GFP+ cells that had dendritic morphology of vertical cells, which are present in deeper layers and extend their dendrites vertically. In the AVCN and PVCN, GFP+/GAD67−

neurons (open squares in Fig. 1B) showed various dendritic morphologies, suggesting that several cell types were labeled.

A dense GFP+ axonal plexus from labeled CN neurons was found in the contralateral ICC. In both cases 10-66 and 10-67, the main plexus was found in the ventral and dorsal part of the ICC, respectively. In case 10-68, labeled axons were spread throughout the ICC, but were most dense in the middle of dorso-ventral axis. Only a few fibers were seen in the ipsilateral IC (not shown). Terminals of GFP+ fibers were immunopositive for VGLUT2. In the contralateral IC, GFP+/VGLUT2+ terminals made contacts on cell bodies of LG neurons (confirmed by 13 deconvoluted stacks, Fig. 4A, B). The axosomatic terminals are most likely to arise only from the DCN since AVCN and PVCN neurons co-express VGLUT1 and VGLUT2 (Ito et al., 2011) and terminals containing both proteins were shown previously not to make axosomatic endings on LG cells (Ito et al., 2009). The majority of LG neurons that received axosomatic contacts from GFP+/VGLUT2+ terminals were found in the ICC (Fig. 2B; Table 4). The number of LG neurons receiving axosomatic contacts was the highest in case 10-66, which showed labeling of the ventral plexus, and the lowest in case 10-67, which showed labeling of the dorsal plexus.

NLL injection cases—After large injections of the virus into the NLL (Table 1), GFP+ neurons were found in the dorsal, intermediate, and ventral nucleus of the lateral lemniscus (DNLL, INLL, and VNLL) (Fig. 1C; Table 5) with a few infected neurons in surrounding non-auditory nuclei. Both GAD67+ and GAD67− neurons were infected with the virus.

GFP+ fibers from infected NLL neurons were found in the ipsilateral IC in cases 11-09, 13-80, and 14-16. In case 11-22, the injections were made bilaterally in the INLL, and GFP+ fibers were found bilaterally in the IC. Labeled fibers were sparsely distributed throughout the IC. In the ICC, labeled axons made laminar plexuses. Terminals of GFP+ axons contained VGLUT2 or GAD67. GFP+/VGLUT2+ terminals made contacts on LG cell bodies (confirmed by 16 deconvoluted stacks, Fig. 4C, D). The LG neurons receiving axosomatic contacts were sparse and were located in all subdivisions of the IC (Fig. 2C; Table 5).

Analysis of axonal terminals from all sources on LG cell bodies

To compare the morphology of single axons contacting the LG neurons, we reconstructed LG cell bodies and GFP+ axons in 3D from high-magnification Z-stack images of the cells and their surrounding structures (Fig. 5A–F). Fifty-three axons (16 SOC, 19 DCN, and 18 NLL) were found in 40 Z-stack images of LG neurons obtained from thirteen rats. In 29 stacks (7 SOC, 8 DCN, 14 INLL), LG cell bodies received a contact from only one axon, while in 11 stacks (4 SOC, 5 DCN, 2 NLL) LG cell bodies received contacts from two or three axons. LG cell bodies received either *en passant* boutons (Fig. 5B, D) or terminal boutons (Fig. 5A, C, E, F).

Terminals from the ascending fibers are larger (Fig. 5C–F) than those from local IC axons (Fig. 5A, B, Ito and Oliver, 2014). The volume of the axon terminals from the SOC, DCN, and NLL axons was significant larger than that of the IC axons ($P = 0.003$, $P < 0.001$, and $P < 0.001$, respectively; Kruskal-Wallis multiple comparison test). The median of volume of

single terminals from the IC, SOC, DCN, and NLL were 2.36, 3.80, 6.16, and 4.13 μm^3, respectively (Fig. 5G).

If one assumes that each labeled axon found in a Z-stack originated from a different neuron, one can calculate the number of contacts per input axon. Single axons from the SOC made 1–5 contacts (median: 1); axons from DCN made 1–4 contacts (median: 2); and axons from the NLL made 1–7 contacts (median: 1.5; Fig. 5H). The mean number of contacts per cell made by axons from each source was not statistically significant ($P = 0.53$, Kruskal-Wallis test; Fig. 5H). If each labeled axon in the same Z-stack originates from the same neuron, the estimated number of contacts made by an axon from SOC, DCN, and NLL is 1–5 (median: 3), 1–8 (median: 4), and 1–7 (median: 2), respectively. The former gives the lowest estimate, while the latter gives the highest estimate. In either case, we can conclude that a single excitatory neuron makes only a few axosomatic terminals on a single LG neuron. This indicates that an LG neuron must receive axosomatic inputs from many excitatory neurons in the brainstem.

Since the number of axosomatic contacts made by a single axon was unrelated to the origin of the axon, the average number of axosomatic excitatory inputs was estimated by dividing the total number of VGLUT2+ axosomatic terminals by the number of GFP+/VGLUT2+ axosomatic terminals which arose from a single neuron. LG cells were reconstructed in 3D and had a mean diameter of 15.97 ± 2.48 μm (mean ± SD, N = 40 LG cells) calculated from the volume of the cell bodies. These neurons were encircled by 189.4 ± 101.6 (mean ± SD) VGLUT2+ axosomatic terminals on average. This distribution was similar for when the GFP + axons in a Z-stack were assumed to originate from different neurons (Fig. 5I) and when they were assumed to originate from a single neuron (Fig. 5J). The LG neurons with a larger surface area received more axosomatic inputs. Indeed, the generalized linear models of the two distributions were $y = 0.08\ x^{1.03}$ and $y = 0.04\ x^{1.10}$, where x and y were surface area and number of inputs, respectively. To assess whether the models described the distribution better than a linear model, which assumed that the number of inputs obeyed a normal distribution, or a null model, which assumed that the number of inputs was not associated with the surface area, we used the Akaike's information criterion (Akaike, 1973) of which smaller value indicates a better model. The Akaike's information criterion of the models were 482.1 and 466.7, and smaller than those of linear models (499.5 and 498.9) or null models (487.8 and 472.0). This suggests that the generalized linear models described the given distribution better than other models. Thus, the number of axosomatic inputs was almost proportional to the surface area of LG cell bodies. Since the surface area of an LG cell body was highly correlated with the square of the mean diameter ($R^2 = 0.808$), we concluded that larger LG neurons have a greater convergence of axosomatic excitatory inputs.

Convergence of inputs from multiple sources on single LG cells

The findings above showed that neurons in the SOC, DCN, and INLL made axosomatic excitatory contacts on LG cells, and many axons converged on a single LG cell. However, the extent to which a single LG cell receives inputs from multiple source nuclei is unclear.

To address this question, we made large lesions of the brainstem nuclei that supply the axosomatic terminals to the LG neurons. If an LG cell receives inputs exclusively from one nucleus, the obvious ring of VGLUT2+ excitatory axosomatic terminals ("axosomatic rings") on the LG cell body should disappear or be severely disrupted after a large lesion in that source, and the number of the axosomatic rings should decline. We made kainic acid injections either in the IC, INLL, DCN, or SOC, the major sources of LG axosomatic excitatory inputs. The injections produced a profound loss of neurons in the target structures (Figs. 6, 7A). The almost complete loss of neurons in the ICC (Fig. 6A, E), INLL (Fig. 6B, F), and SOC (Fig. 6D, K) was indicated by the absence of the immunoreactivity for MAP2 or NeuN visible on the intact side. After DCN injections (Fig. 6C), a few small neurons, presumably granule cells, persisted (Fig. 6G, H). Few, if any large, NeuN-positive large neurons remained on the side of the injection (compare Fig. 6G, H to Fig. 6I, J). Stereological analysis of all cases revealed that the number of neurons in the injected nuclei was significantly reduced in comparison to the intact side ($P < 0.05$; *t*-test; Fig. 7A). About half of the neurons were eliminated by kainic acid (IC, 55.1%; INLL, 64.8%; DCN, 50.4%; SOC, 74.9%; average of 3 cases).

In the IC of animals that received kainic acid lesions in the brainstem, there was a modest reduction of VGLUT2+ terminals. In contrast, after lesions in the ipsilateral IC, VGLUT2+ terminals were sparse (Fig. 7A). Since most remaining VGLUT2+ terminals in these cases were large, it is likely that they originated from the SOC, DCN, and INLL. After lesions in the contralateral IC, the "axosomatic VGLUT2+ rings" were never eliminated completely. Likewise, after lesions in the lower brainstem nuclei, the "axosomatic rings" were not eliminated on either side of the IC (Fig. 7B–G). When counts of "axosomatic rings" were made in the IC, the mean number decreased in the experimental relative to control ICs only after lesions in the ipsilateral IC ($P = 0.008$; *t*-test; Fig. 7H); however, that decrease may reflect the elimination of both LG cells and other IC neurons. In contrast, there was no significant decrease in the number of "axosomatic rings" ($P > 0.13$; Fig. 7H) after lesions in the other locations. These results suggest that few LG cells receive an exclusive input from one extrinsic source.

An LG neuron may receive axosomatic contacts from both local IC axons and from brainstem sources since local excitatory neurons in IC make extensive local collaterals and innervate many LG neurons within the same IC layer (Ito and Oliver, 2014). To test whether there is convergence of inputs from local and ascending sources on a single LG cell, we made injections of palGFP Sindbis virus bilaterally into the IC and injections of pal-mRFP Sindbis virus bilaterally into the SOC (N = 5; Fig. 8A) or unilaterally into the CN (N = 1; Table 1). Both GFP+ and mRFP+ axonal plexuses were found in the IC. LG cells were identified by large MAP2-positive somata surrounded by a high density of VGLUT2+ axosomatic endings, and they received axosomatic contacts from both GFP+/VGLUT2+ and mRFP+/VGLUT2+ terminals (Fig. 8B–F). This innervation pattern was found in all 6 cases examined (N = 16 LG cells) and shows that the same LG neuron can receive converging axosomatic inputs from both local IC neurons and ascending fibers.

Discussion

In the present study, we demonstrated that the LG neurons in the IC receive axosomatic excitatory inputs from neurons in lower brainstem auditory nuclei, i.e. the DCN, SOC, and the INLL in addition to those in the local and commissural IC which were shown to make inputs on LG neurons in a previous study (Ito and Oliver, 2014). Each excitatory input neuron appears to contribute only a small fraction of the dense axosomatic terminals on an LG neuron. Thus, LG neurons may receive converging excitatory ascending inputs from dozens of neurons, and the number of inputs is proportional to the surface area of LG cell bodies. The present data also show the convergence of local and lemniscal inputs on an LG cell body.

Origins of VGLUT2+ terminals from the lower auditory brainstem

Our relatively large virus injections in the SOC, CN, and NLL (Fig. 1) demonstrate the existence of axosomatic inputs from these regions to the LG neurons. Because of the large injections, it may be difficult to identify the contributions of specific subnuclei (Fig. 1; Tables 3–5). Nevertheless, previous observations can clarify some of these contributions. VGLUT2 is a specific marker for the axosomatic terminals on the LG cells (Ito et al., 2009). Brainstem neurons that express the genes for both VGLUT1 and VGLUT2, or make these proteins, are unlikely sources of the VGLUT2+ axosomatic terminals (Ito and Oliver, 2010). For example, the VCN can be eliminated since almost all of these glutamatergic neurons express both the genes for VGLUT1 and VGLUT2 (Ito et al., 2011; Ito and Oliver, 2010). Both proteins are found in the VCN projections to the SOC (Billups, 2005), and the terminals in IC that are double-labeled for these proteins are not axosomatic on LG neurons (Ito et al., 2009).

In the CN, the DCN is the most likely source of VGLUT2+ axosomatic terminals. The fusiform and giant cells are the only neurons in the DCN that express VGLUT2 but not VGLUT1 (Ito et al., 2011; Ito and Oliver, 2010), and these are the most likely sources of the axosomatic LG input. Indeed, a previous study observed tectothalamic neurons that received axosomatic contacts from cochlear nuclear axons (Oliver et al., 1999). The number of those axosomatic contacts ranged from 1 to 5 (average 3). This previous finding is consistent with the present results (Fig. 5H) since LG cells are tectothalamic (Ito et al., 2009) and have a similar number of axosomatic contacts from DCN. LG cells receiving CN excitatory axons were also found in the ICD adjacent to the ICC. This pattern is consistent with previous observations in which DCN axons target the ICC and deep layer of the ICD in the cat (Oliver, 1984).

The SOC is one source of bilateral axosomatic inputs to LG neurons. A substantial number of SOC neurons that express only the message for VGLUT2, but not VGLUT1, send their axons to the IC. These include neurons in the contralateral and ipsilateral LSO, ipsilateral MSO, ipsilateral ventromedial periolivary nucleus, and contralateral lateral nucleus of the trapezoid body (Ito and Oliver, 2010). Glycinergic projection neurons in the LSO co-express GAD67 (Tanaka and Ezure, 2004), and can be ruled out as sources for excitatory axosomatic synapses. LG cells receiving SOC excitatory inputs were mainly found in the lateral ICC and fewer in the cortex of IC. Since neurons in the MSO and LSO almost exclusively target

the ICC (Oliver et al., 1995; Shneiderman and Henkel, 1987), in the IC cortices the GFP+/VGLUT2+ terminals on the LG cells probably arise from periolivary nuclei rather than from LSO or MSO.

The INLL is the most likely source of axosomatic terminals on the LG neurons from the NLL. Most INLL neurons (60%) express only VGLUT2 (Ito and Oliver, 2010), while the proportion of glutamatergic neurons in the other nuclei of the lateral lemniscus is tiny (3–7% of neurons). Furthermore, our observation is consistent with a previous study in which the terminal field of INLL was found to be more extensive in the dorsal cortex than that of the VNLL (Whitley and Henkel, 1984).

Functional implications

Physiological studies of identified GABAergic neurons are just beginning, so it is difficult to know precisely how LG cells differ from small GABAergic and glutamatergic IC neurons. Geis and Borst (2013) found the LG neurons in the ICD have low input resistance and short-latency, excitatory inputs. These properties are consistent with the notion that they provide short-latency, feed-forward inhibition to the thalamus. Presumably, the large number of axosomatic excitatory synapses helps to counteract a large membrane capacitance due to the cell size. Excitatory axosomatic inputs are seldom seen on other IC neuron types (Altschuler et al., 2008).

In the auditory system, axosomatic synapses from multiple neurons are seen in cell types which preserve timing information. For example, in globular bushy cells, which receive many axosomatic excitatory inputs (Spirou et al., 2005), convergence of inputs enhance the phase-locking seen in the auditory nerve (Joris and Smith, 2008). Since LG cells have features that are likely to enhance temporal precision (Geis and Borst, 2013), the activation of excitatory axosomatic terminals on LG neurons may lead to the generation of short-latency, well-time responses. However, a synchronized activation of many glutamatergic inputs would be necessary to drive the LG neuron because of the low input resistance (Geis and Borst, 2013) and large membrane capacitance due to the cell size. The present observations suggest that the somatic surface area of an LG neuron will predict the number of axosomatic synapses on that neuron. Thus, the density of axosomatic synapses per square micron of surface is rather constant despite the substantial size difference among the LG neurons (10–30 μm in diameter). This data further supports the notion that the axosomatic inputs are a specialization that allows the LG cell to overcome a large membrane capacitance.

The conditions that activate the LG cell are still unknown. Single excitatory axons contribute only a few axosomatic synapses to each LG neuron and may be insufficient to drive the cell. Whether axosomatic synapses operate independently or in concert with axodendritic excitatory synapses is not known since their relationship is unclear. Axosomatic and axodendritic inputs may or may not come from the same sources. Based on the current results, stimuli that activate both ascending and local inputs simultaneously are most likely to produce suprathreshold EPSPs suitable for driving the LG cells. Although both ascending and local excitatory inputs converge on the somata of the LG neuron (the present study, Ito and Oliver, 2014), they may not have an equal effect. The ascending axons from the

brainstem have larger axosomatic terminals than those of the local axons. Since larger terminals contain more synaptic vesicles docked with the active zone (Schikorski and Stevens, 1997) and have a higher release probability (Holderith et al., 2012), synapses from ascending fibers may have a higher release probability than those from the local fibers.

The LG neurons appear to be part of a fast, short-latency pathway for inhibition of the MGB. These neurons have the largest axons in the brachium of the IC (Saint Marie et al., 1997), and those axons conduct action potentials to the medial geniculate faster than excitatory neurons in vitro (Peruzzi et al., 1997). Although the LG cells in IC receive inputs from several brainstem inputs, the direct inputs from DCN and outputs to the ventral division of the medial geniculate body (DCN-LG-MGV) would constitute a particularly fast pathway for thalamic inhibition. This is comparable to the CN pathway that projects directly to the medial division of the medial geniculate body (MGM) (Malmierca et al., 2002), but the CN-MGM pathway does not preserve frequency information. The characteristics of the DCN-LG-MGV pathway are consistent with fast, feed-forward inhibition that may arrive at the medial geniculate before excitation from the IC and may be important to control the onset of thalamic firing.

Substantial numbers of medial geniculate neurons receive inhibition from LG neurons in the IC (Bartlett and Smith, 1999; Bartlett and Smith, 2002; Lee and Sherman, 2010; Venkataraman and Bartlett, 2013). A mixture of excitation and inhibition in the medial geniculate body was more prevalent than pure excitation or pure inhibition after focal IC activation (Lee and Sherman, 2010). However, in some cases, the inhibitory and excitatory inputs originated from separate areas in IC. This raises the interesting prospect that the GABAergic LG neurons and the glutamatergic neurons in the same IC lamina may not always share the same postsynaptic target in the thalamus.

Acknowledgments

The authors gratefully acknowledge Drs. Munenori Ono (University of Connecticut Health Center), Nobuaki Tamamaki (Kumamoto University), and Kouichi Nakamura (Oxford University) for their critical reading, Drs. Yugo Fukazawa (University of Fukui) and Hiroshi Kuba (Nagoya University) for helpful discussions, and Dr. Duck O. Kim (University of Connecticut Health Center) for his donation of equipment. This work was supported by grants from Ministry of Education, Science and Culture of Japan (Grant number: 22700365 and 25430034, TI; 24500408 and 25123709, HH; 13J01992, JS; 23115101 and 25250006, TK), the Uehara Memorial Foundation (TI), the Ichiro Kanehara Foundation (TI), NOVARTIS Foundation for the Promotion of Science (TI), Research and Education Program for Life Science of University of Fukui (TI), and NIH R01 DC00189 (DLO).

Abbreviation list

+	positive
−	negative
AVCN	anteroventral cochlear nucleus
BIC	brachial nucleus of the inferior colliculus
CN	cochlear nucleus
DCN	dorsal cochlear nucleus

DNLL	dorsal nucleus of the lateral lemniscus
GAD67	glutamic acid decarboxylase 67kDa
GFP	green fluorescent protein
IC	inferior colliculus
ICC	central nucleus of the inferior colliculus
ICD	dorsal cortex of the inferior colliculus
ICL	lateral cortex of the inferior colliculus
ICR	rostral cortex of the inferior colliculus
INLL	intermediate nucleus of the lateral lemniscus
LG	large GABAergic
LSO	lateral superior olive
mRFP	monomeric red fluorescent protein
MSO	medial superior olive
NLL	nuclei of the lateral lemniscus
PVCN	posteroventral cochlear nucleus
SOC	superior olivary complex
VGLUT	vesicular glutamate transporter
VNLL	ventral nucleus of the lateral lemniscus

Literature cited

Akaike, H. Information theory and an extension of the maximum likelihood principle. Petrov, BN., Caski, F., editors. Budapest; 1973. p. 267-281.

Altschuler RA, Tong L, Holt AG, Oliver DL. Immunolocalization of vesicular glutamate transporters 1 and 2 in the rat inferior colliculus. Neuroscience. 2008; 154(1):226–232. [PubMed: 18436385]

Bartlett EL, Smith PH. Anatomic, intrinsic, and synaptic properties of dorsal and ventral division neurons in rat medial geniculate body. J Neurophysiol. 1999; 81(5):1999–2016. [PubMed: 10322042]

Bartlett EL, Smith PH. Effects of paired-pulse and repetitive stimulation on neurons in the rat medial geniculate body. Neuroscience. 2002; 113(4):957–974. [PubMed: 12182900]

Billups B. Colocalization of vesicular glutamate transporters in the rat superior olivary complex. Neurosci Lett. 2005; 382(1–2):66–70. [PubMed: 15911123]

Fujiyama F, Furuta T, Kaneko T. Immunocytochemical localization of candidates for vesicular glutamate transporters in the rat cerebral cortex. J Comp Neurol. 2001; 435(3):379–387. [PubMed: 11406819]

Furuta T, Tomioka R, Taki K, Nakamura K, Tamamaki N, Kaneko T. In vivo transduction of central neurons using recombinant Sindbis virus: Golgi-like labeling of dendrites and axons with membrane-targeted fluorescent proteins. J Histochem Cytochem. 2001; 49(12):1497–1508. [PubMed: 11724897]

Geis HR, Borst JG. Large GABAergic neurons form a distinct subclass within the mouse dorsal cortex of the inferior colliculus with respect to intrinsic properties, synaptic inputs, sound responses, and projections. J Comp Neurol. 2013; 521(1):189–202. [PubMed: 22700282]

Hioki H, Nakamura H, Ma YF, Konno M, Hayakawa T, Nakamura KC, Fujiyama F, Kaneko T. Vesicular glutamate transporter 3-expressing nonserotonergic projection neurons constitute a subregion in the rat midbrain raphe nuclei. J Comp Neurol. 2010; 518(5):668–686. [PubMed: 20034056]

Holderith N, Lorincz A, Katona G, Rozsa B, Kulik A, Watanabe M, Nusser Z. Release probability of hippocampal glutamatergic terminals scales with the size of the active zone. Nat Neurosci. 2012; 15(7):988–997. [PubMed: 22683683]

Ito T, Bishop DC, Oliver DL. Two classes of GABAergic neurons in the inferior colliculus. J Neurosci. 2009; 29(44):13860–13869. [PubMed: 19889997]

Ito T, Bishop DC, Oliver DL. Expression of glutamate and inhibitory amino acid vesicular transporters in the rodent auditory brainstem. J Comp Neurol. 2011; 519(2):316–340. [PubMed: 21165977]

Ito T, Hioki H, Nakamura K, Tanaka Y, Nakade H, Kaneko T, Iino S, Nojyo Y. Gamma-aminobutyric acid-containing sympathetic preganglionic neurons in rat thoracic spinal cord send their axons to the superior cervical ganglion. J Comp Neurol. 2007; 502(1):113–125. [PubMed: 17335042]

Ito T, Oliver DL. Origins of Glutamatergic Terminals in the Inferior Colliculus Identified by Retrograde Transport and Expression of VGLUT1 and VGLUT2 Genes. Front Neuroanat. 2010; 4:135. [PubMed: 21048892]

Ito T, Oliver DL. The basic circuit of the IC: tectothalamic neurons with different patterns of synaptic organization send different messages to the thalamus. Front Neural Circuits. 2012; 6:48. [PubMed: 22855671]

Ito T, Oliver DL. Local and commissural IC neurons make axosomatic inputs on large GABAergic tectothalamic neurons. J Comp Neurol. 2014; 522(15):3539–3554. [PubMed: 24796971]

Joris PX, Smith PH. The volley theory and the spherical cell puzzle. Neuroscience. 2008; 154(1):65–76. [PubMed: 18424004]

Kataoka N, Hioki H, Kaneko T, Nakamura K. Psychological stress activates a dorsomedial hypothalamus-medullary raphe circuit driving brown adipose tissue thermogenesis and hyperthermia. Cell Metab. 2014; 20(2):346–358. [PubMed: 24981837]

Kemmer M, Vater M. Functional organization of the dorsal cochlear nucleus of the horseshoe bat (Rhinolophus rouxi) studied by GABA and glycine immunocytochemistry and electron microscopy. Anat Embryol (Berl). 2001; 203(6):429–447. [PubMed: 11453161]

Lee CC, Sherman SM. Topography and physiology of ascending streams in the auditory tectothalamic pathway. Proc Natl Acad Sci U S A. 2010; 107(1):372–377. [PubMed: 20018757]

Magnusson AK, Park TJ, Pecka M, Grothe B, Koch U. Retrograde GABA signaling adjusts sound localization by balancing excitation and inhibition in the brainstem. Neuron. 2008; 59(1):125–137. [PubMed: 18614034]

Malmierca MS, Merchan MA, Henkel CK, Oliver DL. Direct projections from cochlear nuclear complex to auditory thalamus in the rat. J Neurosci. 2002; 22(24):10891–10897. [PubMed: 12486183]

Mugnaini, E., Oertel, W. An atlas of the distribution of GABAergic neurons and terminals in the rat CNS as revealed by GAD immunohistochemistry. In: Bjorklund, A., Hokfelt, T., editors. Handbook of chemical neuroanatomy. New York: Elsevier; 1985.

Mullen RJ, Buck CR, Smith AM. NeuN, a neuronal specific nuclear protein in vertebrates. Development. 1992; 116(1):201–211. [PubMed: 1483388]

Nishino E, Yamada R, Kuba H, Hioki H, Furuta T, Kaneko T, Ohmori H. Sound-intensity-dependent compensation for the small interaural time difference cue for sound source localization. J Neurosci. 2008; 28(28):7153–7164. [PubMed: 18614685]

Oliver DL. Dorsal cochlear nucleus projections to the inferior colliculus in the cat: a light and electron microscopic study. J Comp Neurol. 1984; 224(2):155–172. [PubMed: 19180810]

Oliver DL, Beckius GE, Shneiderman A. Axonal projections from the lateral and medial superior olive to the inferior colliculus of the cat: a study using electron microscopic autoradiography. J Comp Neurol. 1995; 360(1):17–32. [PubMed: 7499562]

Oliver DL, Kuwada S, Yin TC, Haberly LB, Henkel CK. Dendritic and axonal morphology of HRP-injected neurons in the inferior colliculus of the cat. J Comp Neurol. 1991; 303(1):75–100. [PubMed: 2005240]

Oliver DL, Ostapoff EM, Beckius GE. Direct innervation of identified tectothalamic neurons in the inferior colliculus by axons from the cochlear nucleus. Neuroscience. 1999; 93(2):643–658. [PubMed: 10465448]

Papadeas ST, Halloran C, McCown TJ, Breese GR, Blake BL. Changes in apical dendritic structure correlate with sustained ERK1/2 phosphorylation in medial prefrontal cortex of a rat model of dopamine D1 receptor agonist sensitization. J Comp Neurol. 2008; 511(2):271–285. [PubMed: 18785628]

Peruzzi D, Bartlett E, Smith PH, Oliver DL. A monosynaptic GABAergic input from the inferior colliculus to the medial geniculate body in rat. J Neurosci. 1997; 17(10):3766–3777. [PubMed: 9133396]

Saint Marie RL, Baker RA. Neurotransmitter-specific uptake and retrograde transport of [3H]glycine from the inferior colliculus by ipsilateral projections of the superior olivary complex and nuclei of the lateral lemniscus. Brain Res. 1990; 524(2):244–253. [PubMed: 1705464]

Saint Marie RL, Stanforth DA, Jubelier EM. Substrate for rapid feedforward inhibition of the auditory forebrain. Brain Res. 1997; 765(1):173–176. [PubMed: 9310410]

Schikorski T, Stevens CF. Quantitative ultrastructural analysis of hippocampal excitatory synapses. J Neurosci. 1997; 17(15):5858–5867. [PubMed: 9221783]

Shneiderman A, Henkel CK. Banding of lateral superior olivary nucleus afferents in the inferior colliculus: a possible substrate for sensory integration. J Comp Neurol. 1987; 266(4):519–534. [PubMed: 2449472]

Spirou GA, May BJ, Wright DD, Ryugo DK. Frequency organization of the dorsal cochlear nucleus in cats. J Comp Neurol. 1993; 329(1):36–52. [PubMed: 8454725]

Spirou GA, Rager J, Manis PB. Convergence of auditory-nerve fiber projections onto globular bushy cells. Neuroscience. 2005; 136(3):843–863. [PubMed: 16344156]

Tamamaki N, Nakamura K, Furuta T, Asamoto K, Kaneko T. Neurons in Golgi-stain-like images revealed by GFP-adenovirus infection in vivo. Neurosci Res. 2000; 38(3):231–236. [PubMed: 11070189]

Tanaka I, Ezure K. Overall distribution of GLYT2 mRNA-containing versus GAD67 mRNA-containing neurons and colocalization of both mRNAs in midbrain, pons, and cerebellum in rats. Neurosci Res. 2004; 49(2):165–178. [PubMed: 15140559]

Venkataraman Y, Bartlett EL. Post-Natal Development of Synaptic Properties of the GABAergic Projection from Inferior Colliculus to Auditory Thalamus. J Neurophysiol. 2013; 109(12):2866–2882. [PubMed: 23536710]

Wallace MN, Shackleton TM, Palmer AR. Morphological and physiological characteristics of laminar cells in the central nucleus of the inferior colliculus. Front Neural Circuits. 2012; 6:55. [PubMed: 22933991]

Whitley JM, Henkel CK. Topographical organization of the inferior collicular projection and other connections of the ventral nucleus of the lateral lemniscus in the cat. J Comp Neurol. 1984; 229(2):257–270. [PubMed: 6501602]

Winer JA, Saint Marie RL, Larue DT, Oliver DL. GABAergic feedforward projections from the inferior colliculus to the medial geniculate body. Proc Natl Acad Sci U S A. 1996; 93(15):8005–8010. [PubMed: 8755593]

Young, ED., Oertel, D. Cochlear nucleus. In: Shepard, GM., editor. The synaptic organization of the brain. 5. Oxford: Oxford University Press; 2004. p. 125-163.

Zufferey R, Donello JE, Trono D, Hope TJ. Woodchuck hepatitis virus posttranscriptional regulatory element enhances expression of transgenes delivered by retroviral vectors. J Virol. 1999; 73(4):2886–2892. [PubMed: 10074136]

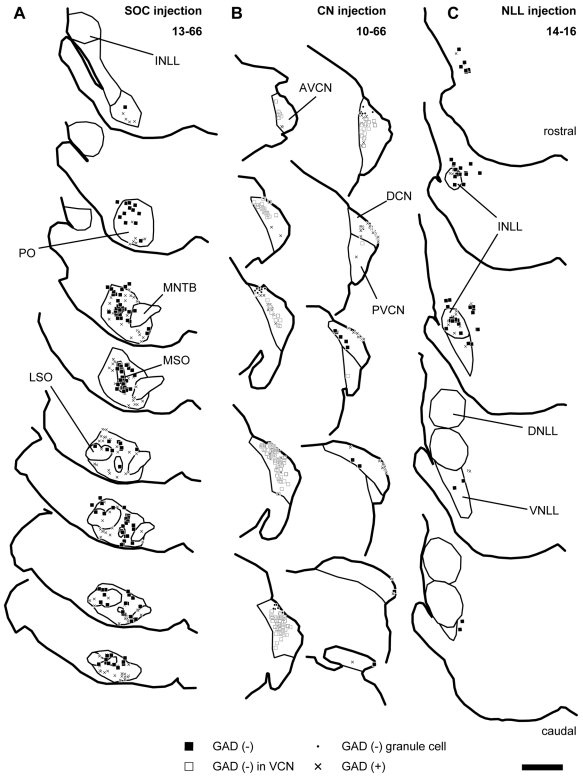

Figure 1.

Traces of injection sites of recombinant viruses. Filled squares indicate GFP+ neurons negative for GAD67; "**x**", GFP+ neurons positive for GAD67; open squares, GFP+ VCN neurons negative for GAD67; dots, GFP+/GAD67− neurons in the granule cell domain of the CN. (**A**) An example of SOC injection cases (13-66). Infected neurons were distributed throughout the SOC. The few infected cells outside of the SOC were not in auditory nuclei. (**B**) An example of CN injection cases (10-66). Infected neurons were found in the DCN, AVCN, and PVCN. (**C**) An example of INLL injection cases (14-16). Infected neurons were mainly found in the INLL and the surrounding regions. Each trace is separated by 240 μm. Scale bar: 1 mm. Abbreviations: AVCN, anteroventral cochlear nucleus; DCN, dorsal cochlear nucleus; DNLL, dorsal nucleus of the lateral lemniscus; INLL, intermediate nucleus of the lateral lemniscus; LSO, lateral superior olive; MSO, medial superior olive; MNTB, medial nucleus of the trapezoid body; PO, periolivary nucleus; PVCN, posteroventral cochlear nucleus; VNLL, ventral nucleus of the lateral lemniscus.

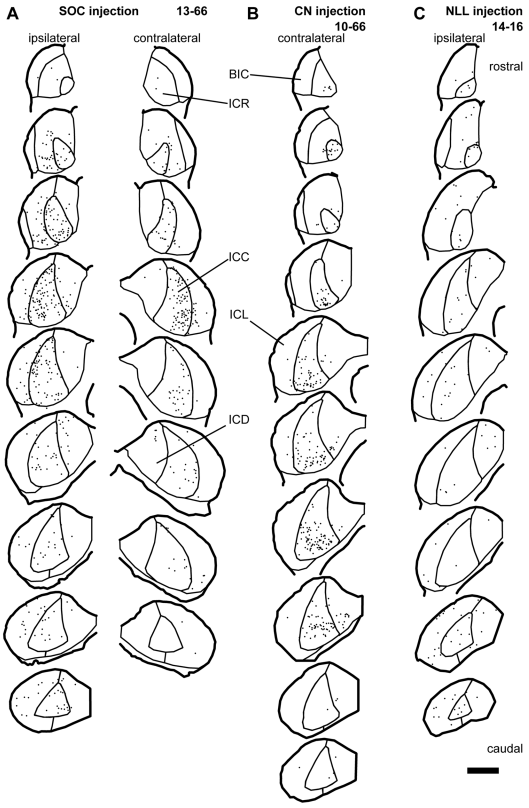

Figure 2.

Distribution of LG cells (dots) which received axosomatic contacts with GFP+/VGLUT2+ terminals. (**A**) An SOC injection case (13-66). LG cells receiving contact were found bilaterally. In the ICC, LG cells receiving contact were located mainly in the lateral part. (**B**) A CN injection case (10-66). LG cells receiving contact were mainly found in the ICC of the contralateral side. (**C**) An NLL injection case (14-16). LG cells receiving contact were sparsely distributed throughout the IC of the ipsilateral side. Each trace is separated by 240 μm. Scale bar: 1 mm. Abbreviations: BIC, brachial nucleus of the IC; ICC, central nucleus of the IC; ICD, dorsal cortex of the IC; ICL, lateral cortex of the IC; ICR, rostral cortex of the IC.

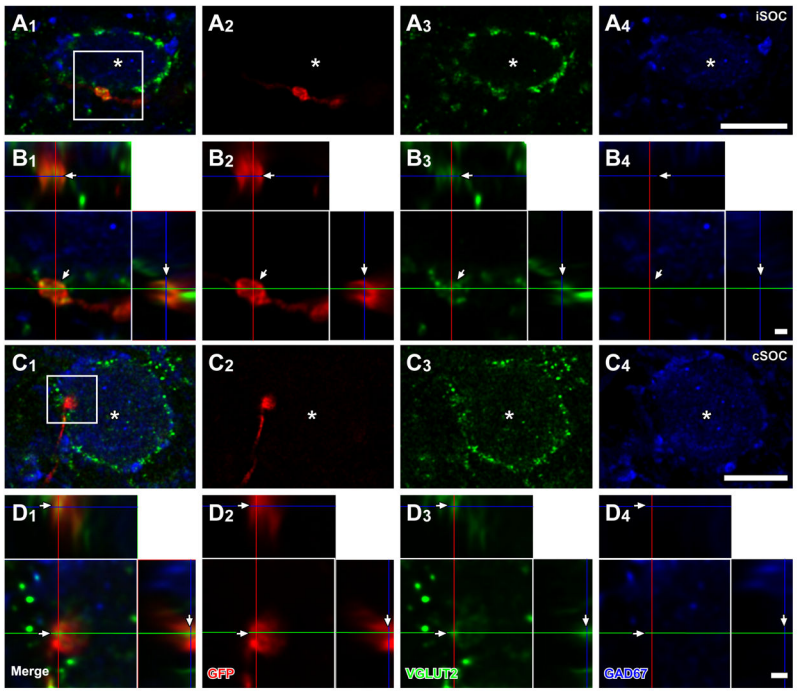

Figure 3.

LG cells receive axosomatic excitatory inputs from bilateral SOC. After an injection of palGFP Sindbis virus in the hemilateral SOC, LG cells (blue, asterisks) with GFP+ (red) terminals, which were also positive for VGLUT2 (green), were found in the ipsilateral (**A, B**) and contralateral (**C, D**) IC. Case 10-60. (**B, D**) High-magnification images of a box in $\mathbf{A_1}$ and $\mathbf{C_1}$ with orthogonal views of the stack cut at 3 planes parallel to xy- (blue lines), yz- (a red line), and xz-planes (a green line). GFP+/VGLUT2+ terminals made contact on LG cells (arrows). Scale bars: 10 μm (**A, C**), and 1 μm (**B, D**). Three-dimensional reconstructions of these GFP+ axons and LG cell bodies are shown in Fig. 5.

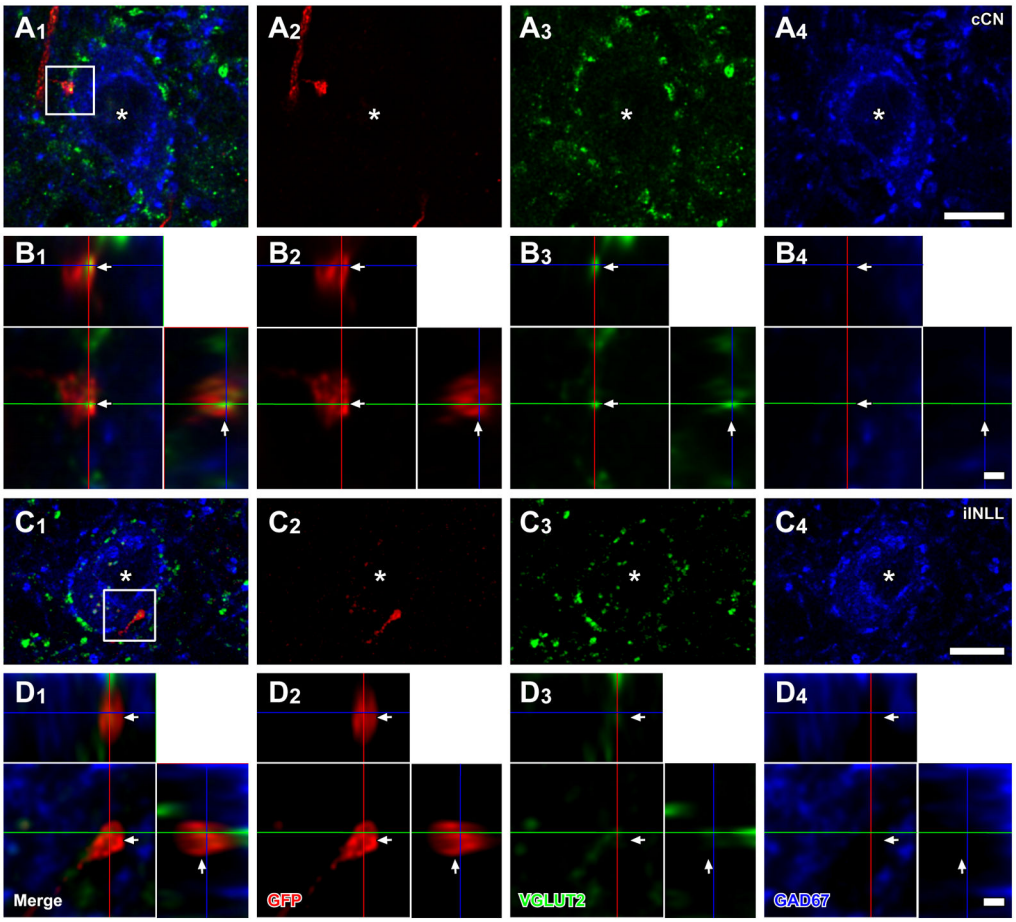

Figure 4.

LG cells receive axosomatic excitatory inputs from the cochlear nuclei and INLL. LG cells (blue, asterisks) with GFP+ (red) terminals, which colocalized VGLUT2 immunoreactivity (green), were found after an injection of palGFP Sindbis virus in the contralateral CN (case 10-68; **A, B**), or ipsilateral INLL (case 11-22; **C, D**). (**B, D**) High-magnification images of a box in $\mathbf{A_1}$ and $\mathbf{C_1}$ with orthogonal views of the stack cut at 3 planes parallel to xy- (blue lines), yz- (a red line), and xz-planes (a green line). GFP+/VGLUT2+ terminals made contact on LG cells (arrows). Scale bars: 10 μm (**A, C**), and 1 μm (**B, D**). Note that three-dimensional reconstructions of these GFP+ axons and LG cell bodies are shown in Fig. 5.

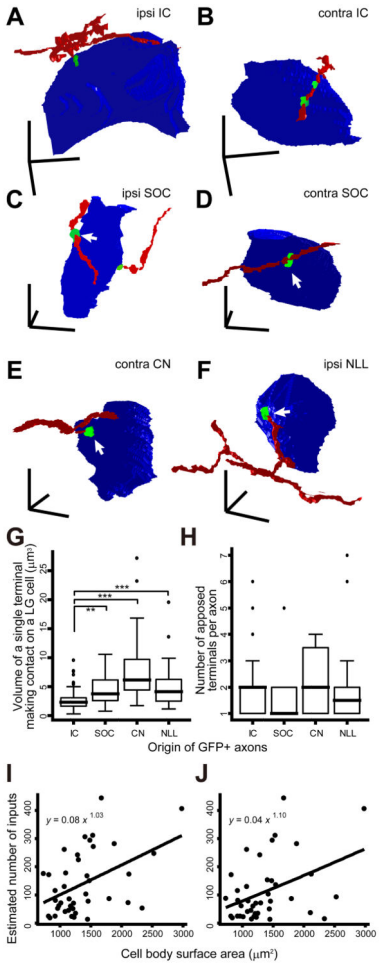

Figure 5.

Single axons made only a few axosomatic contacts on a single LG cell. (**A–F**) Three-dimensional reconstruction of GFP+ axons (red), GFP+/VGLUT2+ terminals (green), and LG neural cell bodies (blue). (**A, B**) LG cells and IC glutamatergic axons that terminate on the LG cell bodies, which are the reprint from **Fig. 9B, C** of Ito and Oliver (2014). (**C**) An LG cell shown in Fig. 3A, which was found in the ipsilateral side to the injected SOC. (**D**) An LG cell shown in Fig. 3B, which was found in the contralateral side to the injected SOC. (**E**) An LG cell shown in Fig. 4A, which was found in the contralateral side to the injected CN. (**F**) An LG cell shown in Fig. 4C, which was found in the ipsilateral side to the injected NLL. Arrows indicate the same terminals shown in Figs. 3 and 4. Note that terminals from lower nuclei (**C–F**) are larger than IC excitatory axosomatic terminals (**A, B**). Scale bars: 10 μm. (**G, H**) The volume of a single GFP+/VGLUT2+ terminal which made contact on a single LG cell body (**G**) and number of axosomatic contacts (**H**) by a single GFP+ axonal branch originated from the IC, SOC, CN, or INLL. Data of IC were from Ito and Oliver (2014). Thick horizontal bars indicate medians. Top and bottom horizontal hinges of boxes indicate 1st and 3rd quartiles, respectively. Circles are the outliers, and whiskers indicate the maximum and minimal values after eliminating outliers. The number of apposed terminals made by a single axon from the different sources was not significantly different ($P = 0.53$,

Kruskal-Wallis multiple comparison test). On the other hand, volume of a single terminal that arose from IC neurons was significantly smaller than that from neurons in other nuclei. Asterisks indicate the pair showing significant difference ($P < 0.05$ for *, $0.05 < P < 0.01$ for **, and $0.01 < P < 0.001$ for ***, Kruskal-Wallis test). (**I, J**) The number of axosomatic inputs was almost proportional to the surface area of LG cell bodies. Estimated number of inputs, which was calculated by dividing total number of VGLUT2+ axosomatic terminals by number of GFP+/VGLUT2+ axosomatic terminals that arose from a single axon (**I**) or all axons (**J**) in a Z-stack. The fitting curves were calculated under a generalized linear model.

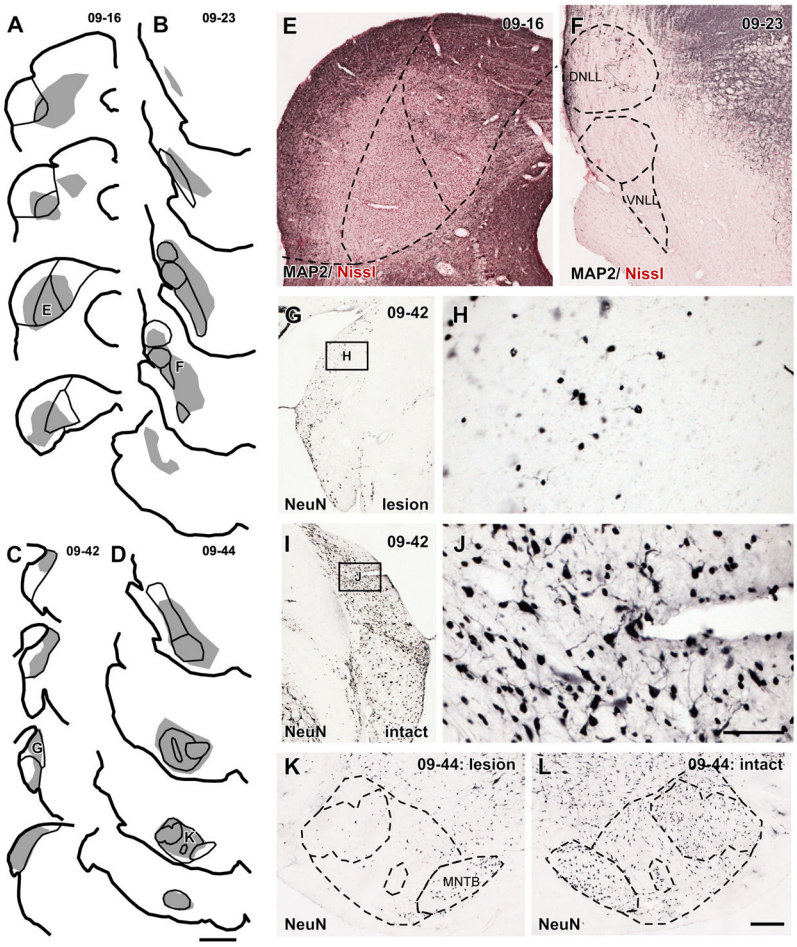

Figure 6.

(**A–D**) Injection sites of kainic acid. Shaded area indicates sites with marked neuronal loss. (**A**) A case in which injection was made in the ICC (case 09-16). Neuronal loss was observed in the ICD and ICL as well. A trace with “E” is the same section as **E**. (**B**) A case in which injection was made in the INLL (case 09-23). Neuronal loss was observed in whole nuclei of the lateral lemniscus. A trace with “F” is the same section as **F**. (**C**) A case in which injection was made in the DCN (case 09-42). A trace with “G” is the same section as **G**. (**D**) A case in which injection was made in the SOC (case 09-44). Almost complete loss of neurons was obtained except for the MNTB. A trace with “K” is the same section as **K**. Each trace is separated by 480 μm. (**E**) A photomicrograph of the injection site of an IC injection case. MAP2+ neurons disappeared in the center of the IC. Counterstained with Neutral-Red. (**F**) A photomicrograph of the injection site of an INLL injection case. Almost complete loss of MAP2+ neurons in the nuclei of the lateral lemniscus. Counterstained with Neutral-Red. (**G**) A photomicrograph of the injection site of a DCN injection case. (**H**) A higher magnification of a box in **G**. Only small NeuN+ neurons, presumably granule cells, were found. (**I**) A photomicrograph of the intact side of the DCN of the same case of **G**. (**J**) A higher magnification of a box in **I**. Both large and small NeuN+ neurons were observed. (**K**) A photomicrograph of the injection site of a SOC injection case. Almost complete loss of NeuN+ neurons except for the MNTB. (**L**) A photomicrograph of the intact side of a SOC

of the same case of **K**, showing normal cytoarchitecture of the complex. Scale bars: 1 mm (**A–D**), 300 μm (**E, F, G, I, K, L**), and 60 μm (**H, J**).

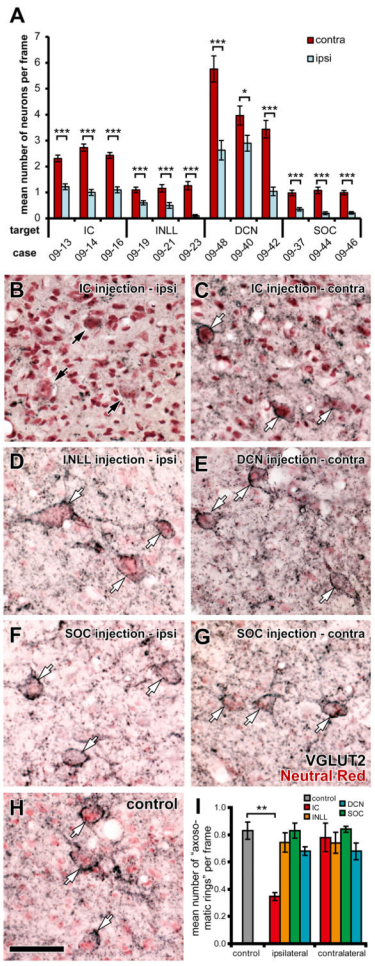

Figure 7.

VGLUT2+ axosomatic endings are still present after a single injection of kainic acid in contralateral IC, unilateral INLL, SOC, or DCN. (**A**) Average number of neurons, which was identified with NeuN or MAP2 labeling, in a counting frame was significantly decreased in the nuclei that received kainic acid injection than the contralateral nuclei in all cases examined (*t*-test; *, $P = 0.031$; ***, $P < 0.001$). Error bars indicate the standard errors of mean. In SOC cases, the MNTB was excluded from counting since the nucleus does not project to the IC. (**B**) In the ipsilateral ICD of a case which received kainic acid injection in the ICC (case 09-16), although several large cells (black arrows), which were counterstained with Neutral-Red (pink), were found, they were not encircled by dense VGLUT2+ terminals (black). Note that fine VGLUT2+ terminals found in the other panels (**C–H**) were almost absent in **B**. (**C**) Many presumable LG cells (white arrows) were identified in the contralateral ICC of the same case. (**D**) Axosomatic endings on large cells (white arrows) were present after an injection of kainic acid in the ipsilateral INLL (case 09-23). (**E**) Axosomatic endings on large cells (white arrows) were present after an injection of kainic acid in the contralateral DCN (case 09-42). (**F, G**) Axosomatic endings on large cells (white arrows) were present bilaterally after an injection of kainic acid in the SOC (case 09-44). (**H**) Axosomatic endings on large cells (white arrows) in control ICC. Scale bar: 50 μm. All

images were taken in the ICC except for **B**, which was taken in the ICD because of complete disappearance of MAP2-immunoreactivity in the ipsilateral ICC of case 09-16 (Fig. 6E). (**I**) Mean number of presumed LG cells per a sampling frame. Significant decrease of the number to control ($P = 0.008$, *t*-test) was detected only in the ipsilateral IC (injection site). Error bars indicate standard error of the mean.

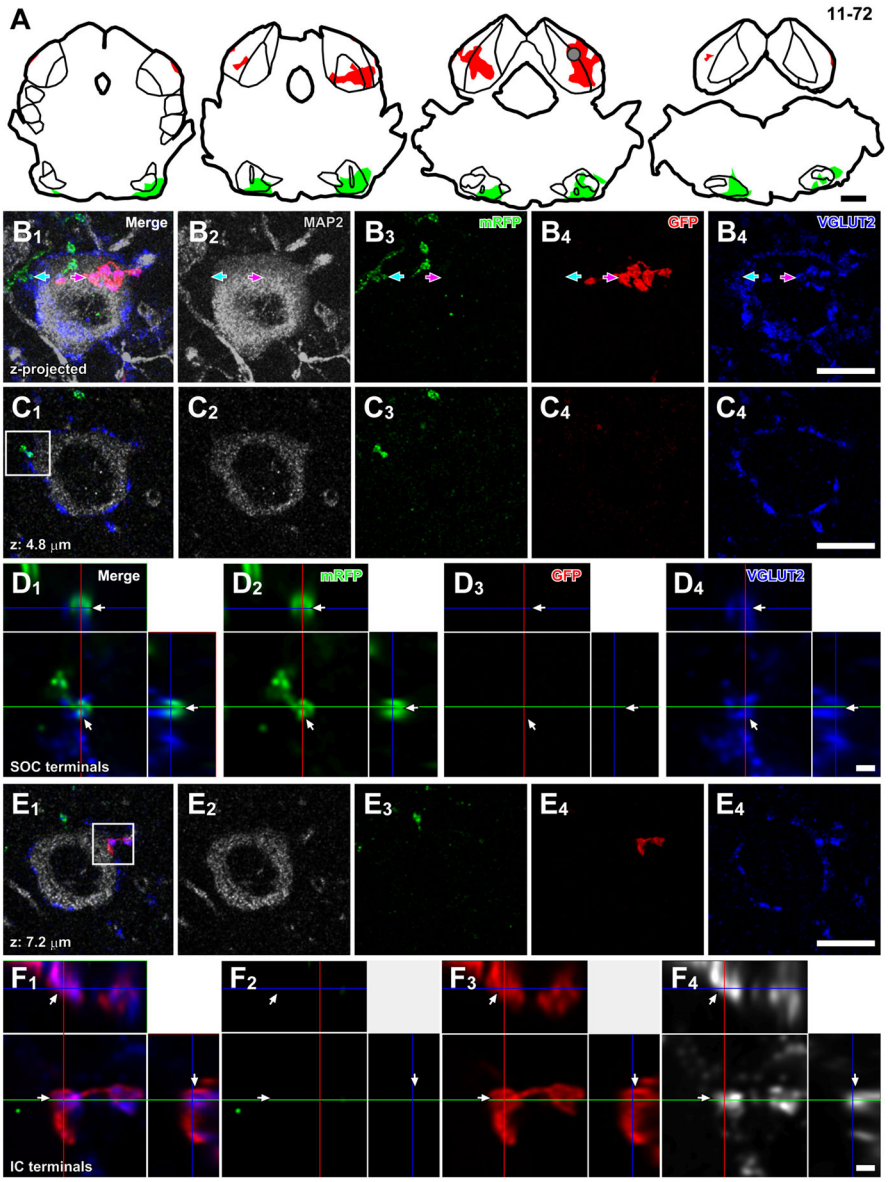

Figure 8.

Convergence of axons from lower brainstem nuclei and local neurons on a single LG cell. (**A**) Injection sites of palGFP Sindbis (red) and Sindbis pal-mRFP (green) viruses of case 11-72. Each trace was separated by 480 μm. A gray circle indicates approximate location of the LG cell in **B–F**. (**B**) Maximal projection of Z-stack images of a putative LG cell, which had MAP2+ cell body (gray) with dense VGLUT2+ axosomatic endings (blue), receiving axosomatic contact with both GFP+ (red arrows) and mRFP+ terminals (green arrows). The projection image was made from 23 Z-stack images, in which each image was separated by 0.48 μm. (**C**) A single Z-plane image showing axosomatic contact between mRFP+ terminals (green) and the LG cell body (gray). (**D**) A high-magnification image of a box in **C$_1$** with orthogonal views of the stack cut at 3 planes parallel to xy- (blue lines), yz- (a red line), and xz-planes (a green line). The terminal positive for both mRFP (green) and

VGLUT2 (blue) was indicated by arrows. (**E**) A single Z-plane image showing axosomatic contact between GFP+ terminals (red) and the LG cell body (gray). (**F**) A high-magnification image of a box in $\mathbf{E_1}$ with orthogonal views of the stack. The terminal positive for both GFP (red) and VGLUT2 (blue) was indicated by arrows. Scale bars: 1 mm (**A**), 10 μm (**B, C, E**), and 1 μm (**D, F**).

J Comp Neurol. Author manuscript; available in PMC 2017 May 27.

Table 1

Animals that received viral injections. Abbreviations: SOC, superior olivary complex; NLL, nuclei of the lateral lemniscus; CN, cochlear nuclei; IC, inferior colliculus.

	Case #	Location of GFP+ cell bodies		Case #	Location of GFP+ cell bodies	
Sindbis palGFP, a single injection	10-60	SOC		10-66	CN	
	10-61	SOC		10-67	CN	
	11-49	SOC		10-68	CN	
	10-96	NLL		11-21	NLL	
	11-9	NLL		11-22	NLL	
	13-80	NLL				
adeno-associated virus 2/5 palGFP, a single injection	13-66	SOC		14-16	NLL	
Dual injections of Sindbis palGFP and pal-mRFP	11-37	bilateral IC	unilateral CN	11-42	bilateral IC	bilateral SOC
	11-40	bilateral IC	bilateral SOC	11-71	bilateral IC	bilateral SOC
	11-41	bilateral IC	bilateral SOC	11-72	bilateral IC	bilateral SOC

Table 2

Table of primary antibodies used.

Antigen	Description of Immunogen	Source, Host Species, Cat. #, Clone or Lot#, RRID	Concentration Used
Glutamic acid decarboxylase 67 (GAD67)	Recombinant whole protein of rat GAD67.	Millipore, mouse monoclonal, Cat# MAB5406, RRID: AB_2278725.	1:1000
MAP2	Bovine brain microtubule protein (aa 997–1332).	Millipore, mouse monoclonal clone AP20, Cat# MAB3418, RRID: AB_94856.	1:200
NeuN	Purified cell nuclei from mouse brain.	Millipore, mouse monoclonal clone A60, Cat# MAB377, RRID: AB_94966.	1:100
Vesicular glutamate transporter 2 (VGLUT2)	KLH-conjugated, synthetic peptide corresponding to amino acids residues CWPNGWEKKEEFVQESAQDAYS YKDRDDYS of rat VGLUT2 (aa. 554–582).	Professor Takeshi Kaneko (Kyoto University), guinea-pig and rabbit polyclonal.	0.5 μg/ml
Green fluorescent protein (GFP)	Recombinant whole protein of enhanced green fluorescent protein.	Professor Takeshi Kaneko (Kyoto University), guinea-pig and rabbit polyclonal.	0.2 μg/ml
Monomeric red fluorescent protein (mRFP)	Recombinant whole protein of red fluorescent protein.	Professor Takeshi Kaneko (Kyoto University), guinea-pig and rabbit polyclonal.	0.2 μg/ml

Table 3

The number of GFP+ neurons and LG neurons which received contact with terminals positive for both GFP and VGLUT2 in SOC injection cases. MNTB, medial nucleus of the trapezoid body; MSO, medial superior olive; PO, periolivary nuclei; LSO, lateral superior olive; BIC, brachial nucleus of the IC; ICR, rostral cortex of the IC; ICL, lateral cortex of the IC; ICD, dorsal cortex of the IC; ICC, central nucleus of the IC.

injection site		# GFP+ neurons										# LG neurons receiving contact with GFP+/VGLUT2+ terminals											
		GAD67-negative					GAD67-positive					ipsilateral						contralateral					
	case #	MNTB	MSO	PO	LSO	total	MNTB	MSO	PO	LSO	total	BIC	ICR	ICL	ICD	ICC	total	BIC	ICR	ICL	ICD	ICC	total
SOC	10-60	0	3	15	0	18	0	1	3	0	4	0	0	4	0	16	20	0	0	0	0	4	4
	10-61	0	12	7	0	19	0	2	8	0	10	0	0	1	0	46	47	0	2	0	0	4	6
	11-49	32	3	7	0	42	0	0	11	0	11	0	2	2	0	22	26	0	0	0	0	0	0
	13-66	1	23	95	14	133	2	0	109	10	121	2	29	87	35	273	426	0	11	28	9	162	210

Table 4

The number of GFP+ neurons and LG neurons which received contact with terminals positive for both GFP and VGLUT2 in CN injection cases. DCN, dorsal cochlear nucleus; VCN, ventral cochlear nucleus.

injection site		# GFP+ neurons								# LG neurons receiving contact with GFP+/VGLUT2+ terminals					
		GAD67-negative				GAD67-positive				contralateral					
	case #	DCN	VCN	granule cells	total	DCN	VCN	granule cells	total	BIC	ICR	ICL	ICD	ICC	total
CN	10-66	11	149	21	181	32	35	0	67	0	15	18	27	261	321
	10-67	6	10	3	19	42	3	0	45	0	4	5	2	23	34
	10-68	6	26	2	34	14	9	0	23	0	4	15	20	97	136

Table 5

The number of GFP+ neurons and LG neurons which received contact with terminals positive for both GFP and VGLUT2 in NLL injection cases. DNLL, dorsal nucleus of the lateral nucleus; INLL, intermediate nucleus of the lateral lemniscus; VNLL, ventral nucleus of the lateral lemniscus.

injection site		# GFP+ neurons								# LG neurons receiving contact with GFP+/VGLUT2+ terminals					
		GAD67-negative				GAD67-positive				ipsilateral					
	case #	DNLL	INLL	VNLL	total	DNLL	INLL	VNLL	total	BIC	ICR	ICL	ICD	ICC	total
NLL	11-9	0	2	0	2	0	0	0	0	0	0	2	0	7	9
	11-22 [L]	0	1	0	1	0	0	0	0	0	0	2	0	2	4
	11-22 [R]	1	5	0	6	0	1	0	1	0	1	5	0	9	15
	13-80	4	6	0	10	4	1	0	5	0	0	9	0	3	12
	14-16	0	17	4	21	0	11	1	12	2	17	40	21	48	128